Vacancy formation in MoO3: hybrid density functional theory and photoemission experiments

Akande, SO, Chroneos, A, Vasilopoulou, M, Kennou, S & Schwingenschlögl, U

Original citation & hyperlink:
Akande, SO, Chroneos, A, Vasilopoulou, M, Kennou, S & Schwingenschlögl, U 2016, 'Vacancy formation in MoO3: hybrid density functional theory and photoemission experiments' *Journal of Materials Chemistry C Materials for optical, magnetic and electronic devices*, vol 4, no. 40, pp. 9526-9531
https://dx.doi.org/10.1039/C6TC02571D

DOI 10.1039/C6TC02571D
ISSN 2050-7526

Publisher: Royal Society of Chemistrt

Vacancy formation in MoO_3: Density functional theory calculations and photoemission experiments

Salawu Omotayo Akande,[1] Maria Vasilopoulou,[2] Alexander Chroneos,[3,4] Stella Kennou,[5] and Udo Schwingenschlogl[1,*]

[1]*King Abdullah University of Science and Technology (KAUST), Physical Sciences and Engineering Division (PSE), Thuwal 23955-6900, Saudi Arabia*

[2]*Institute of Nanoscience and Nanotechnology (INN), National Center for Scientific Research Demokritos, 15310 Aghia Paraskevi, Athens, Greece*

[3]*Department of Materials, Imperial College, London SW7 2AZ, United Kingdom*

[4]*Faculty of Engineering and Computing, Coventry University, Priory Street, Coventry CV1 5FB, United Kingdom*

[5]*Department of Chemical Engineering, University of Patras, 26500, Patras, Greece*

Abstract

Molybdenum oxide (MoO_3) is an important material that is being considered for numerous technological applications, including catalysis and electrochromism. In the present study, we apply hybrid density functional theory to investigate O and Mo vacancies in the orthorhombic phase. We determine the vacancy formation energies of the different defect sites as functions of the electron chemical potential, addressing different charge states. In addition, we investigate the consequences of defects for the material properties. Ultraviolet photoemission spectroscopy is employed to study the valence band of stoichiometric and O defective MoO_3. We show that O vacancies result in occupied in-gap states.

*Electronic address: udo.schwingenschlogl@kaust.edu.sa,+966(0)544700080

I. INTRODUCTION

MoO_3 is frequently used in Li-ion batteries, electrochromism, heterogenous catalysis, and as cathode material [1–4]. Its ability to activate C-H bonds in alkanes and its role in oxidation reactions in industrial processes, for example, are of great practical importance [5–7]. On the other hand, the usability in electronics and optoelectronics is poor due to the large and indirect band gap. Defects are known to be key for electronic applications of the material, since charge transfer is not feasible in pristine MoO_3 [8]. They also govern the interface and surface reactions in catalysis and electrochromism [9]. Indeed, the usability of MoO_3 in catalysis depends critically on O vacancies, as different Mo oxidation states are provided [10–12]. Besides the possibility to modify the physical properties, the ability to change the oxidation state affects the breaking and formation of bonds with reactants [13]. Furthermore, defects have been reported to enhance the extraction of holes when MoO_3 is used as anode buffer layer in organic photovoltaics [14].

Orthorhombic MoO_3 (space group Pbmn) is a layered material, consisting of bilayers held together by weak van der Waals forces along the [010] direction. The bilayers comprise MoO_6 octahedra that share edges along the [001] direction and vertices along the [100] direction. There exist three distinct O sites: symmetric, asymmetric, and terminal, refer to Figure 1. The symmetric and asymmetric sites are also called bridging sites. The symmetric sites are

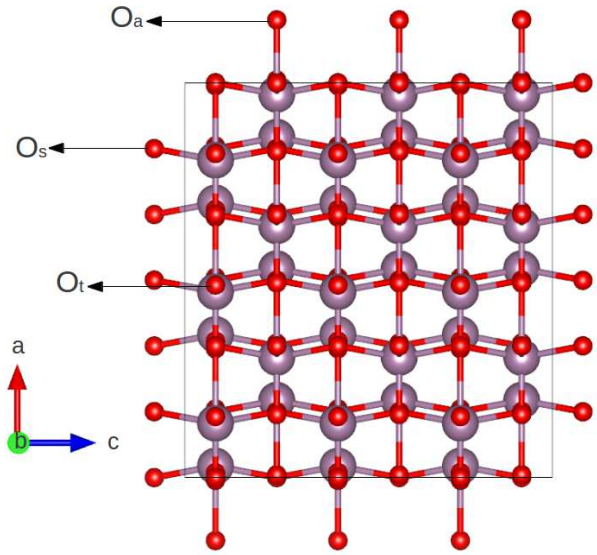

FIG. 1: (Color online) Crystal structure of MoO_3, showing the three O sites.

three-fold coordinated with two shorter (1.95 Å) and one longer (2.33 Å) distance to Mo, the asymmetric sites two-fold coordinated with one shorter (1.73 Å) and one longer (2.25 Å) distance to Mo, and the terminal sites one-fold coordinated with the shortest distance to Mo (1.67 Å). Discrepancies exist in the literature concerning the relative stability of the different O sites. There are experimental and theoretical reports that suggest it would be easier to create O vacancies at bridging sites [15, 16], while controlled oxidation of MoO_3 (110) films rather points to the terminal site [17].

Introduction of native defects can be employed to tune the electronic structure of MoO_3 and induce in-gap states with high density [8]. On the one hand such in-gap states can dramatically enhance the electrical conductance, on the other hand they give rise to high responsivity of photodetection in the visible light range. Since the vacancy formation in MoO_3 and its influence on the material properties remains an open issue, the present study aims at investigating the energetics of vacancies and the consequences of their presence. We will employ density functional theory, as this methodology can provide important insights in the formation of native defects in solid state systems [18]. The obtained electronic structure data will be compared to photoemission experiments.

II. COMPUTATIONAL DETAILS

The following calculations refer to thermally stable orthorhombic MoO_3 and are performed using the projector augmented wave method of the Vienna Ab-initio Simulation Package [19]. A plane wave basis set with cut-off energy 500 eV and a $5 \times 3 \times 5$ Γ-centred k-mesh are used for optimizing $3 \times 1 \times 3$ supercells (144 atoms) of MoO_3 until the residual forces have declined to less than 0.02 Å/eV. Larger supercells are investigated to control finite size effects. In order to evaluate the role of electronic correlations in localized d and f orbitals, both GGA (generalized gradient approximation) and GGA+U calculations are performed, using different U values (Dudarev approach) [20]. Furthermore, for including the interaction between bilayers and issues that will be discussed later, we employ the Heyd-Scuseria-Ernzerhof (HSE06) hybrid functional with van der Waals interaction term added. Atomic charges are calculated by the Bader approach [21].

The formation energy of a defect is related to the Fermi level μ_f and charge q, being

defined as [22]

$$E_{D,q} = E_D + \sum n_\alpha \mu_\alpha + q(E_{VBM} + \mu_f) - E, \quad (1)$$

where E and E_D are the total energies of supercells without and with defect, respectively. Moreover, n_α is the number of atoms of species α removed from or added to the supercell and μ_α is the corresponding chemical potential. The energy of the valence band maximum in the perfect supercell is denoted by E_{VBM}. Since μ_f is measured with respect to E_{VBM}, it ranges from 0 to the value of the band gap. We find that the value of $E_{D,q}$ varies only within 0.05 eV between supercells containing 144 and 258 atoms, which does not affect the trends reported in the following. The growth conditions are defined by μ_α, ranging from O-poor (Mo-rich) to O-rich (Mo-poor). The O chemical potential of MoO_3 cannot exceed that of an O atom in the O_2 molecule in gas phase and the Mo chemical potential cannot exceed that of a Mo atom in the bulk metal.

III. EXPERIMENTAL DETAILS

MoO_3 films are deposited in a home-made deposition system [23, 24] consisting of a stainless steel reactor in that the sample is positioned on an Al susceptor, 2 cm below a heated W filament. The filament temperature is set to 660 °C, controlled by the current using calibration data obtained with a tiny thermocouple mechanically fixed to it. The deposition time is used to control the film thickness. Note that the substrate remains near room temperature during deposition. The base pressure is set to 80 mTorr. We use a commercial pressure stabilization system with diaphragm pressure gage (Baratron) and PC-driven needle valve, allowing for the flow of either O_2 or forming gas (90% N_2 and 10% H_2) through the reactor, thus setting the deposition environment.

The valence band spectra of 10 nm thick MoO_3 films deposited on InSnO substrate either in oxidizing or reducing environment are recorded by ultraviolet photoemission measurements, using the He I (21.22 eV) excitation line. A negative bias of 12.28 V is applied to the samples in order to analyze the high binding energy region and derive the absolute work function. The analyzer resolution is determined from the width of the Au Fermi edge, resulting in 0.16 eV, and the oxide stoichiometry from X-ray photoemission spectra of the Mo 3d core level. The unmonochromatized Mg K_α line at 1253.6 eV (15 keV with 20 mA anode current) and an analyzer (Leybold EA-11) pass energy of 100 eV, giving a full width

at half maximum of 1.3 eV for the Au $4f_{7/2}$ peak, are used in all X-ray photoemission measurements. Finally, the Mo $3d$ spectra are fitted with asymmetric Gaussian-Lorentzian curves.

IV. RESULTS AND DISCUSSION

TABLE I: Lattice parameters and Mo-O distances in MoO_3.

	GGA	GGA+U (4.3 eV)	GGA+U (6.3 eV)	Experiment
a (Å)	3.92	3.89	3.88	3.96
b (Å)	13.67	13.66	13.67	13.86
c (Å)	3.70	3.73	3.75	3.70
Mo-O_s(Å)	1.95 (2×)	1.96 (2×)	1.96 (2×)	1.95 (2×)
	2.40	2.39	2.39	2.33
Mo-O_a(Å)	1.76	1.79	1.80	1.73
	2.18	2.14	2.11	2.25
Mo-O_t(Å)	1.70	1.70	1.70	1.67

The optimized lattice parameters of the MoO_3 unit cell (calculated for a $7 \times 3 \times 7$ Γ-centred k-mesh) reproduce the experimental values within 2%, see Table I, and the Mo-O distances obtained by the GGA and GGA+U (U = 4.3 eV, 6.3 eV) methods within 3.1%, 4.9%, and 6.2%, respectively [8, 25]. Figure 2 addresses the density of states obtained by the GGA, GGA+U (4.3 eV) and HSE06 (relaxed GGA structure) methods. We find in all three cases a valence band of about 6 eV width (in agreement with the experimental situation [8]) that contains primarily the O states, with Mo contributions clearly below the Fermi level. On the other hand, the conduction band is dominated by the Mo states and reflects the covalent nature of the bonding in MoO_3 by a significant hybridization with O states. Despite similar shapes of the density of states, the size of the band gap varies strongly with the calculational approach used. While a value of 2.1 eV is obtained for the GGA method, the GGA+U method yields 1.9 eV and the HSE06 method 3.1 eV (which agrees well with the experimental value of 3.3 eV [25]). Also, the HSE06 method results in a wider valence band than the other two methods (6.3 eV versus 5.8 eV). The GGA and GGA+U methods

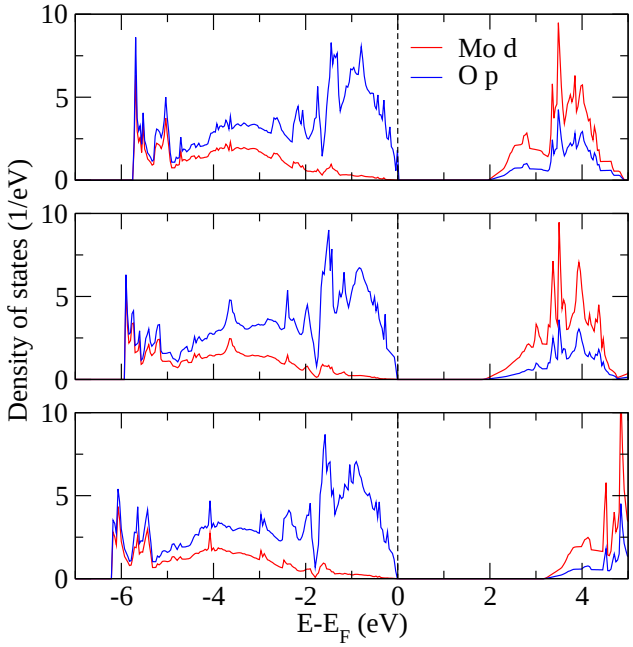

FIG. 2: (Color online) Densities of states of MoO_3 obtained by the GGA (top), GGA+U (4.3 eV) (middle), and HSE06 (bottom) methods.

are well known to underestimate band gaps in related materials.

For the GGA functional we obtain Bader atomic charges of 2.67 for Mo, -1.06 for O_s, -0.93 for O_a, and -0.68 for O_t, all notably lower than the formal charges (Mo^{6+} and O^{2-}). As expected, the Bader charge is more negative when an O atom is involved in more Mo-O bonds. The O vacancy formation energy is calculated using the HSE06 functional and turns out to depend not only on the availability of O in the environment (O-poor or O-rich) but also on the coordination number. It is calculated by removing one O atom from the supercell and adjusting the charge state. The results are presented in Fig. 3 as a function of μ_f. It turns out that the O vacancy formation energy is almost identical for the O_a and O_t sites (irrespective of the charge state of the defect), which is due to the fact that in both cases one short Mo-O double bond is formed, see Table I. On the other hand, we obtain for the O_s site an O vacancy formation energy that is about twice as high. The reason is that we have in this case two Mo-O single bonds instead of one double bond. It previously has been reported for neutral defects on the MoO_3 (010) surface that the difference in the O vacancy formation energy is 0.08 eV between the O_a and O_t sites [9, 26]. The similarity of the two sites is further supported by results from X-ray absorption experiments for the MoO_3 (010) surface [27]. The fact that we obtain not exactly the same values as Ref. [26] can be

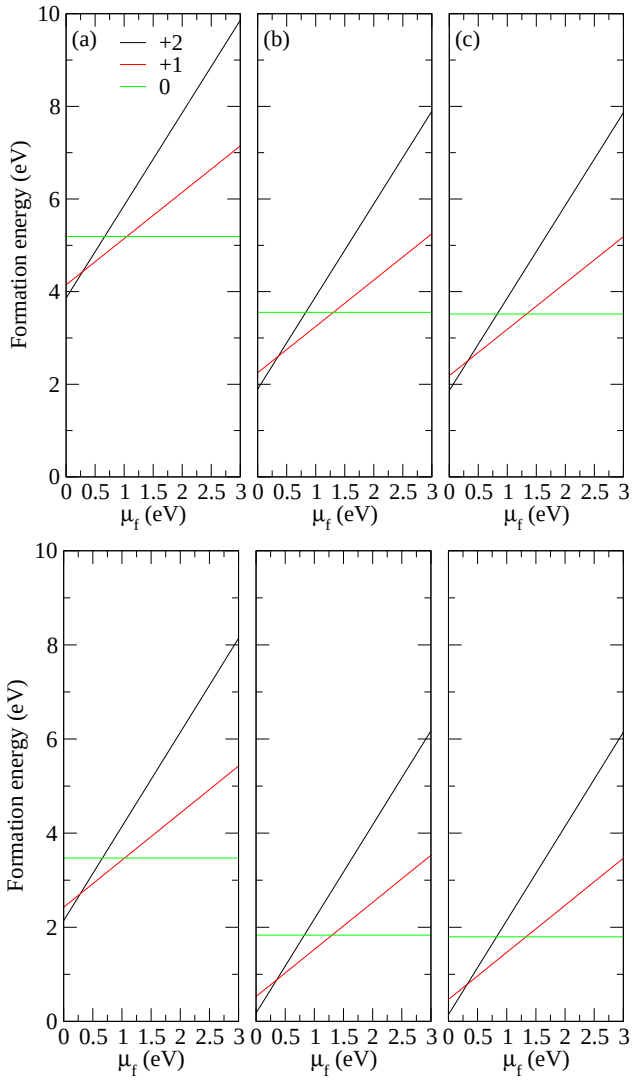

FIG. 3: (Color online) Vacancy formation energies for the (a) symmetric, (b) asymmetric, and (c) terminal O sites. The top row refers to O-rich and the bottom row to O-poor environment.

attributed to the different functionals (GGA and GGA+U) used in the previous work as well as to surface effects. Our value of 3.6 eV for the neutral O_a vacancy agrees reasonably well with the 3.98 eV obtained by Guo and Robertson [28] by the HSE06 functional, given the fact that these authors have used the experimental lattice constants.

For both O-poor and O-rich environment, +2, +1, and 0 charged O_a vacancies form for growing μ_f. For the neutral state and O-rich environment we obtain O vacancy formation energies of 5.18 eV, 3.60 eV, and 3.63 eV for the symmetric, asymmetric, and terminal sites, respectively. O vacancies thus slightly favor asymmetric sites over terminal sites, whereas they are difficult to form on symmetric sites. While the O vacancy formation energies in

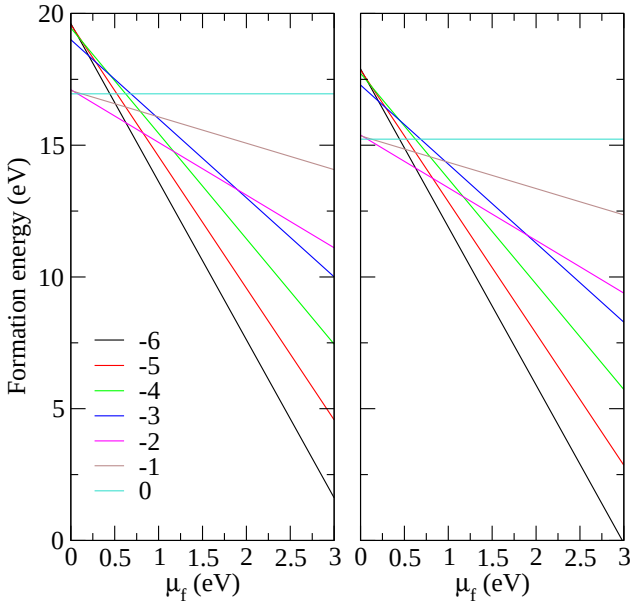

FIG. 4: (Color online) Mo vacancy formation energy in Mo-rich (left) and Mo-poor (right) environment.

O-poor environment are lower, as to be expected, we observe similar trends as in O-rich environment, with the lowest value for the O_a site in the +2 charge state. This conclusion is in qualitative agreement with Ref. [9], however, our values are smaller, because, as stated earlier, the previous study has addressed the MoO_3(011) surface and used the GGA+U functional. In other words, it is more difficult to create an O vacancy on the MoO_3(011) surface than in the bulk [26]. The reduction of metal oxides requires redistribution of the charge of the removed O atoms. In the present case, the released electrons occupy localized Mo d_{xz} in-gap states, see Fig. 5, leaning to the conduction band edge (n-type defect).

Charge states from -6 to 0 are considered for the Mo vacancy both in Mo-poor and Mo-rich environment. As expected, the Mo vacancy formation energies are lower in Mo-poor environment for all charge states. While in a wide range of μ_f the -6 charge state is favorable, see Fig. 4, the -2 charge state is favorable below 0.7 eV and the neutral state below 0.1 eV. For transition metals with octahedral coordination, the crystal field splits the d states into t_{2g} and e_g manifolds, the former giving rise to the conduction band edge and the latter being located at higher energy. Hence, the size of the band gap is determined by the t_{2g} states [29]. Figure 5 (left/middle) shows that the formation of a Mo vacancy leads to localized O p_z in-gap states leaning to the valence band edge (p-type defect), which

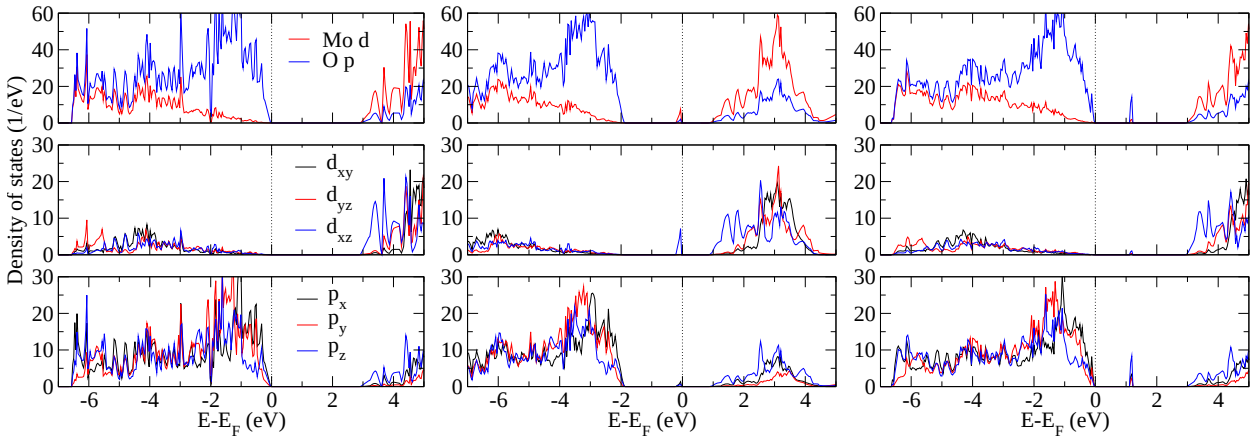

FIG. 5: (Color online) Densities of states of the MoO_3 supercell without vacancy (left), with asymmetric O vacancy (middle), and with Mo vacancy (right). XXXleftnoisy

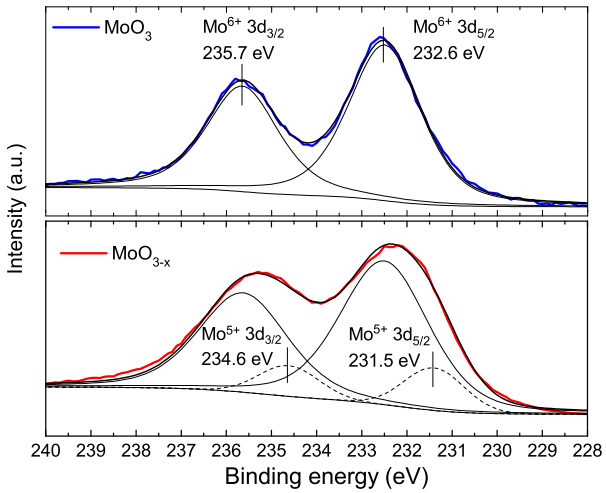

FIG. 6: (Color online) X-ray photoemission Mo 3d core level spectra of MoO_3 and MoO_{3-x} films.

accomodate the introduced holes.

Mo 3d core level spectra are shown in Fig. 6. The spectrum of the film deposited in O_2 environment (termed as MoO_3) consists of a spin-orbit doublet with peaks at 232.6 eV and 235.7 eV binding energy, associated with the Mo^{6+} cations of the fully stoichiometric (oxidized) compound [30–32]. The spectrum of the film deposited in reducing environment (termed as MoO_{3-x}) is considerably broader and the doublet evolves to a less structured shape. The presence of Mo^{5+} cations is evident (Mo $3d_{5/2}$ at 231.5 eV and Mo $3d_{3/2}$ at 234.6 eV binding energy) [33, 34]. It is therefore reasonable to assume that deposition in reducing environment yields an under-stoichiometric sample with O vacancies. Note that it is not

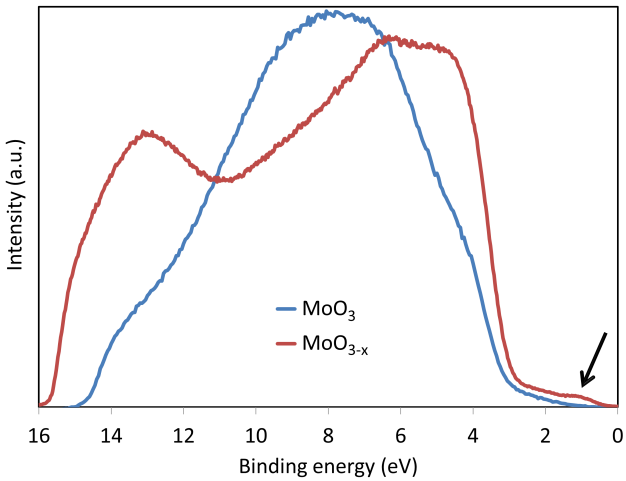

FIG. 7: (Color online) Ultraviolet photoemission (valence band) spectra of MoO_3 and MoO_{3-x} films.

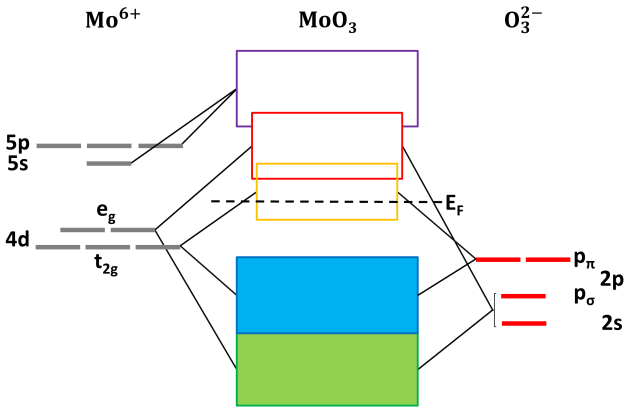

FIG. 8: (Color online) Energy band scheme of MoO_3.

possible to obtain samples containing Mo vacancies by our deposition method.

Ultraviolet photoemission (valence band) spectra of the MoO_3 and MoO_{3-x} films are shown in Fig. 7. The spectrum of the MoO_3 film consists of a single broad peak, as expected for an amorphous sample [35]. The MoO_{3-x} film shows an increased spectral width as well as a new peak appearing above the valence band edge, being indicative of the formation of occupied in-gap states [36], in agreement with our numerical predictions. Comparison of experiment and theory leads to the energy band scheme displayed in Fig. 8. According to the chemical formula, each anionic orbital is to be weighted by a factor three. By symmetry, the anionic p_σ orbitals are stabilized relative to the p_π orbitals by both the electrostatic crystalline field and the covalency of the σ-bond. Therefore, the top of the s-p valence band

has anionic O $2p_\pi$ character, as predicted by our calculations. The bottom of the conduction band, on the other hand, has cationic character, consisting of Mo $3d$ states that are split into e_g and t_{2g} manifolds. The latter have lower energy and thus form the conduction band edge. Absorption measurements for MoO_3 (empty conduction band) demonstrate a wide band gap of 3.0 eV. This value agrees excellently with the results of our hybrid density functional calculations, see Fig. 2. In the case of MoO_{3-x} the additional charge occupies the initially empty t_{2g} states, which partially split off the conduction band edge and give rise to the in-gap states predicted by theory and measured by ultraviolet photoemission spectroscopy.

V. CONCLUSION

We have employed first-principles electronic structure calculations to investigate the formation of O and Mo vacancy defects in MoO_3, using the GGA, GGA+U, and HSE06 functionals. In addition, we have conducted photoemission experiments on stoichiometric and O defective films. The HSE06 functional reproduces the experimental value of the band gap with a deviation of only 0.2 eV and therefore is used for analyzing the defect energetics. It turns out that O is removed much easier from the asymmetric and terminal than from the symmetric sites, which is understood in terms of the involved Mo-O bonds and their respective lengths. As a function of μ_f, +2, +1, and 0 charge states are found to be favorable for O vacancies, while Mo vacancies realize only 0, −2, and −6 charge states. We find that O vacancies are formed easier in bulk MoO_3 than on the MoO_3(011) surface. Both O and Mo vacancies in MoO_3 result in localized in-gap states (n or p-type defects, respectively), while the size of the fundamental band gap is hardly affected.

Acknowledgement

The research reported in this publication was supported by funding from King Abdullah University of Science and Technology (KAUST).

[1] A. Bielanski and J. Haber, Oxygen in Catalysis, Marcel Dekker, New York, 1991.

[2] J. Haber and E. Lalik, Catal. Today, 1991, 33, 119-137.

[3] B. Grzybowska-Swierkosz, Top. Catal. 2000, 23, 11-12.

[4] T. Ressler, J. Wienold, R. Jentoft, and T. Neisius, J. Catal. 2002, 210, 67.

[5] R. K. Grasselli and J. D. Burrington, Adv. Catal. 1981, 30, 133163.

[6] Y. Morooka and W. Ueda, Adv. Catal. 1994, 40, 233273.

[7] O. Lezla, E. Bordes, P. Courtine, and G. Hecquet, Catal. 1997, 170, 346356.

[8] M. Vasilopoulou, A. Douvas, D. Georgiadou, L. Palilis, S. Kennou, L. Sygellou, A. Soultati, I. Kostis, G. Papadimitropoulos, D. Davazoglou, and P. Argitis, J. Am. Chem. Soc. 2012, 134, 16178.

[9] R. Coquet and D. Willock, J. Chem. Chem. Phys. 2005, 7, 3819-3828.

[10] J. Volta and J. Tatibovet, J. Catal. 1985, 93, 467-470.

[11] M. Banares and J. Fiero, Catal. Lett. 1993, 17, 205-211.

[12] M. Chen, C. Friend, and E. Kaxiras, J. Am. Chem. Soc. 2002, 123, 2224-2230.

[13] A. Getsoian and A. Bell, J. Phys. Chem. C, 2013, 117, 25562-25578.

[14] B. Dasgupta, W. Goh, Z. Ooi, L. Wong, C. Jiang, Y. Ren, E. Tok, J. Pan, J. Zhang, and S. Chiam, J. Phys. Chem. C, 2103, 117, 9206-9211.

[15] M. Smith and S. Ozkan, J. Catal. 1993, 141, 124-139.

[16] M. Smith and S. Ozkan, J. Catal. 1993, 142, 226-236.

[17] Y. Lei and Z. Chen, J. Phys. Chem. C 2012, 116, 25757-25764.

[18] M. Youssef and B. Yildiz, Phys. Chem. Chem. Phys. 2014, 16, 1354-1365.

[19] G. Kresse, and D. Joubert, Phys. Rev. B 1999, 59, 1758-1775.

[20] S. Dudarev, G. Botton, S. Savrasov, C. Humphreys, and A. Sutto, Phys. Rev. B 1998, 57, 1505-1509.

[21] G. Henkelman, A. Arnaldsson and H. Jonsson, Comput. Mater. Sci. 2006, 36, 354-360.

[22] A. Janotti and C. G. Van de Walle, Phys. Rev. B 2007, 165202.

[23] M. Vasilopoulou, I. Kostis, N. Vourdas, G. Papadimitropoulos, A. Douvas, N. Boukos, S. Kennou, and D. Davazoglou, J. Phys. Chem. C 2014, 118, 12632-12641.

[24] I. Kostis, N. Vourdas, G. Papadimitropoulos, A. Douvas, M. Vasilopoulou, N. Boukos, D. Davazoglou, J. Phys. Chem. C 2013, 117, 18013-18020.

[25] A. Bouzidi, N. Benramdane, H. Tabet-Derranz, C. Mathieu, B. Khelifa, and R. Desfeux, Mater. Sci. Eng. B 2003, 97, 5-8.

[26] D. Mei, A. M. Karim, and Y. Wang, J. Phys. Chem. C 2011, 115, 8155-8164.

[27] M. Cavalleri, K. Hermann, S. Guimond, Y. Romanyshyn, H. Kuhlenbeck, and H. Freund, Catal. Today 2007, 124, 21-27.

[28] Y. Guo and J. Robertson, Appl. Phys. Lett. 2014, 105, 222110.

[29] P. Huang, Y. He, C. Cao, and Z. Lu, Sci. Rep. 2014, 4, 7131.

[30] W. Criinert, A. Y. Stakheev, R. Feldhaus, K. Anders, E. S. Shpiro, and K. M. Minachev, J. Phys. Chem. 1991, 95, 1323-1328.

[31] M. T. Greiner, M. G. Helander, W.-M. Tang, Z.-B Wang, J. Qiu, and Z.-H. Lu, Nat. Mater. 2012, 11, 76-81.

[32] M. T. Greiner, L. Chai, M. G. Helander, W.-M. Tang, and Z.-H. Lu, Adv. Funct. Mater. 2012, 22, 45574568.

[33] T. H. Fleisch and G. J. Mains, J. Chem. Phys. 1982, 76, 780-786.

[34] A. Katrib, A. Benadda, J. W. Sobczak, and G. Maire, Appl. Catal. A Gen. 2003, 242, 31-40.

[35] F. Werfer and E. Minni, J. Phys. C: Solid State Phys. 1983, 16, 6091-6100.

[36] R. Tokarz-Sbieraj, R. Grybos, and M. Witko, Appl. Catal. A Gen. 2011, 391, 137-143.